UNCLASSIFIED

Defense Technical Information Center Compilation Part Notice

ADP010909

TITLE: Stochastic Subsurface Flow and Transport in Fractal Conductivity Fields

DISTRIBUTION: Approved for public release, distribution unlimited

This paper is part of the following report:

TITLE: Paradigms of Complexity. Fractals and Structures in the Sciences

To order the complete compilation report, use: ADA392358

The component part is provided here to allow users access to individually authored sections of proceedings, annals, symposia, ect. However, the component should be considered within the context of the overall compilation report and not as a stand-alone technical report.

The following component part numbers comprise the compilation report:

ADP010895 thru ADP010929

UNCLASSIFIED

STOCHASTIC SUBSURFACE FLOW AND TRANSPORT IN FRACTAL CONDUCTIVITY FIELDS

ALBERTO S. NDUMU, PAUL S. ADDISON

Civil Engineering Group, School of the Built Environment, Napier University, 10 Colinton Road, Edinburgh, EH10 5DT, Scotland, UK.

Monte Carlo simulations of subsurface flow and contaminant transport of a non-reactive solute plume by steady-state flow with a uniform velocity were performed in a two-dimensional synthetic heterogeneous porous media whose hydraulic conductivity is non-stationary and described by multi-scale fractional Brownian motion. Analysis of the flow and transport results indicates that the longitudinal velocity variance is nearly constant in the longitudinal direction while in the transverse direction it assumes a parabolic shape. The velocity variance is maximum at the impervious boundaries and decreases in transverse direction with distance from the boundaries reaching the minimum value at the domain centre. We observe that the particle displacement covariance is anomalous or non-Fickian at all times t in the dispersion process irrespective of the Hurst exponent H and grows temporally faster than linearly.

1 Introduction

Natural variability of subsurface (i.e., hydrologic and geologic systems) hydraulic properties is the main factor controlling the flow and spreading of contaminants in subsurface porous media. The primary physical property which exhibits large-scale natural spatial variability is the hydraulic conductivity. One important source of error in numerical models to simulate flow and transport in the subsurface stems from lack of knowledge concerning the spatial variability of hydraulic conductivity. In practice, we typically have sparse data which is inadequate to completely describe the spatial variability. This is a consequence of the high data collection cost required to fully characterise a given subsurface porous medium. Hence, the variation of subsurface hydraulic conductivity cannot generally be described in all its detail and is therefore uncertain[1].

One response to the problem of the uncertainty of subsurface hydraulic conductivity has been an interest in stochastic methods, which provide a formal framework for the treatment of uncertainty. Spatial variability of subsurface properties is such that their unique, deterministic, description is not feasible[2], and this is formally recognised in the stochastic approach, in which subsurface hydraulic conductivity is commonly regarded as a random scalar field (RSF).

Stochastic theories involve the description of the local porous medium structure using a statistical model that requires a small number of parameters to be identified from field measurements. The detailed spatial distribution of logconductivity is conventionally reduced to a few statistical parameters, for example, covariance function, mean, variance, and correlation length. It thus follows that the outputs from stochastic models are probabilistic, characterised, for example, by the statistical moments or the full probability density function of the variable of interest.

In this study, we perform Monte Carlo experiments by generating a large number of independent random conductivity realisations with a fractal semivariogram function, solving the stochastic boundary value problem by repetitively solving a set of

deterministic flow problems, each of which is an equally probable representation of the response of the real heterogeneous medium. The flow problem is solved by employing a block-centred finite difference scheme (e.g., Smith and Freeze[3]) to obtain subsurface velocity fields. A random walk particle tracking algorithm is used to solve the transport equation (e.g.,[4-7]) using realised velocity fields. Realised solutions are averaged to get fluctuating log conductivity semivariograms, velocity variances, particle displacement covariance and mean solute concentrations.

2 Random Field Model

In the Monte Carlo simulation of subsurface flow and transport, the first step is the choice of the statistical model that represents the medium heterogeneity, mainly the log hydraulic conductivity, $\ln K(\mathbf{x})$. Most stochastic theoretical and numerical modelling approaches (see e.g.[7-9]) assume that the log hydraulic conductivity $Y(\mathbf{x}) = \ln K(\mathbf{x})$ where $K(\mathbf{x})$ is the local hydraulic conductivity of the subsurface porous medium and $\mathbf{x}$ is the vector of spatial co-ordinates, as stationary random scalar field, normally distributed and characterised by a constant mean $\langle Y \rangle$ and isotropic exponential covariance functions e.g., $C_Y(r) = \sigma_Y^2 e^{-r/\lambda}$ (with $r = |\mathbf{r}|$, where $\mathbf{r}$ is the two-point isotropic lag, σ_Y^2 is the variance of the distribution, and λ the finite integral scale). The justification for using this model is based on geostatistical data obtained from several sites (e.g.,[10]). In addition, the macrodispersivity measured from tracer tests agree approximately well with the stochastic theory results based on the exponential model. Zhan and Wheatcraft[11] argue that, field hydraulic conductivity measurements are limited, have large uncertainty and have been carried out for relatively small spatial scales (at most a kilometre). If the measurements are available at much larger spatial scales, conductivity values may remain correlated at larger scales and may give rise to *non-stationary fractal* or *self-similar* distributions[12-14] with infinite correlation length. Neuman[15] proposes a spatial scaling assumption with a semivariogram function given in (1) to describe such a distribution as

$$\gamma_Y(r) = \frac{1}{2}\left\langle \left[Y(\mathbf{x}+\mathbf{r}) - Y(\mathbf{x})\right]^2 \right\rangle = \gamma_0 (r/\lambda)^{2H}, \tag{1}$$

where λ is a reference scale, γ_0 is a constant variance parameter, and the scaling exponent H is the Hurst exponent[16]. Equation (1) has been demonstrated to be valid for self-affine stochastic processes over the broad range $0 < H < 1$[24]. The exponent H is associated with the fractal dimension $D_S = E + 1 - H$, where E is the space dimensionality. For $0 < H < 1$ the variance and integral scale of the field Y grow infinitely, thus describing a medium with spatially evolving heterogeneity. The semivariogram, given by (1), shows a continuous growth with distance. The presence of more than one reference scale of variability has an influence on fluid flow and contaminant migration[6]. Spatially evolving scale formations are characterised by a variance which keeps growing with the domain size. For a bounded domain, the order of magnitude of the variance is given from (1) by the following:

$$\sigma_Y^2 = \gamma_0 R^{2H}, \tag{2}$$

where R is the characteristic dimension of the domain (upper fractal cut-off scale). Hence, the log conductivity integral scale λ shows the following scaling property:

$$\lambda \propto \alpha R \tag{3}$$

where α is a constant that depends on H. For independent realisations of the log conductivity field, the variance of the random processes varies because of lack of stationarity. However, averaging over many realisations, the order of magnitude of the variance is controlled by the above relationship. The spatial variability of the field is controlled by H while, for a given H, the contrast existing between the actual values of log conductivity Y is controlled by γ_0. Increasing γ_0, keeping H constant, amplifies the contrast between block conductivites. To perform hydraulic conductivity simulations for different H values, the same order of magnitude of the fluctuations needs to be maintained. This was needed in order to obtain realistic fluctuations for the case $H > 1/2$. From a practical point of view we impose in all cases the following condition:

$$\gamma_0 R^{2H} = \sigma_Y^2, \tag{4}$$

where σ_Y^2 is the variance of the field at the maximum size of the modelled domain (upper cut-off scale). This means that once we fix the value γ_0 for the case $H < 1/2$, say $[\gamma_0]_1$ for $H = H_1$, the coefficient $[\gamma_0]_2$ for the case $H = H_2 > 1/2$ becomes:

$$[\gamma_0]_2 = \frac{[\gamma_0]_1 R^{2H_1}}{R^{2H_2}}. \tag{5}$$

Field measurements of hydraulic conductivity have indicated an approximately log-normal distribution[10]. The same distribution has therefore been adopted for the simulations generated in this study. Essentially, a normally distributed log conductivity field $Y(x,y)$ of stationary increments and isotropic semivariogram given in (1) is generated over a two-dimensional domain, the hydraulic conductivity field is obtained by the transformation

$$K(x,y) = \exp[Y(x,y)], \tag{6}$$

where $K(x,y)$ is the conductivity assigned to the point x,y of the domain. The turning band method[19,20] was used to simulate the hydraulic conductivity fields. Using this approach we do not require to filter the wavelengths larger than the field dimension (fractal cut-off scale), from the Y spectrum. The larger scale of variability is limited by the field dimension, and the cut-off is introduced by the fact that the generation is performed in a finite domain similar to the work of Bellin *et al.*,[6]. Since the log conductivity field Y is non-stationary, the mean value of Y is maintained constant in each realisation of the field Y, by conditioning the field to a given constant value[21]. This

translates to conditioning the mean velocity field to a given constant value. Figure (1a) and (1b) shows two realised fractal hydraulic conductivity fields generated using the turning bands method. The simulated fields pertain to $H = 0.3$, and $H = 0.8$ respectively. These fields show dramatically different behaviour. When $H > 1/2$, Y is positively correlated and the fields shows smooth variations and large-scale persistence[22] of the positive and negative values, Fig. 1b. Conductivity values tend to cluster above or below the mean for quite some distance before they change to the other side of the mean. When $H < 1/2$, Y is negatively correlated and leads to less persistence within the conductivity values, and hence Y varies erratically, Fig.1a.

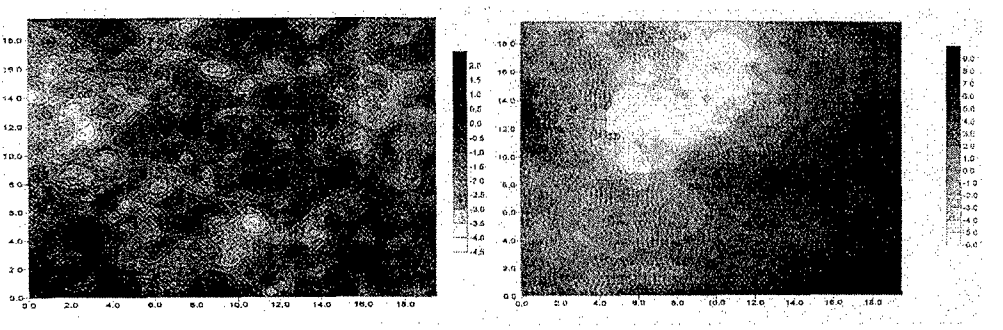

(a) $H = 0.3$ (b) $H = 0.8$

Figure 1: Fractal Hydraulic Conductivity Fields Simulated by Turning Bands Method.

To address model accuracy, we consider the following statistic:

$$\gamma_Y^s(\mathbf{r}) = \frac{1}{2N}\sum_{j=1}^{N}\left[Y(\mathbf{x}_j) - Y(\mathbf{x}_j - \mathbf{r})\right]^2 \tag{7}$$

where N denotes the number of pairs of log hydraulic conductivity Y with separation equal to r. $\gamma_Y^s(\mathbf{r})$ is the semivariogram obtained by spatial averaging all the equi-distant pairs in a single realisation over a single replicate and assuming stationarity. The reconstructed expected value of the log conductivity semivariograms for $H = 0.3, 0.8$, are shown in Figure (2a) and (2b) respectively. The expected values are computed in a Monte Carlo sense averaging over a number of MC independent realisations as

$$\gamma_Y^{MC}(\mathbf{r}) = \left\langle \gamma_Y^s(\mathbf{r}) \right\rangle = \frac{1}{MC}\sum_{j=1}^{MC}\gamma_Y^{s,(j)}(\mathbf{r}) \tag{8}$$

according to the following convergence criteria[6]

$$\left\{\frac{1}{M}\sum_{k=1}^{M}\left[\gamma_Y^{MC}(\mathbf{r}_k) - \gamma_Y^{MC-1}(\mathbf{r}_k)\right]^2\right\}^{/2} \le \varepsilon, \tag{9}$$

where $\mathbf{r}_k$ is the distance of the two point lag along the North-South (NS) and East-West (EW) directions of the modelled domain and M is the number of points used to discretise the semivariogram. The simulated and theoretical semivariograms (Eq. (1)) along NS (squares) and EW (triangles) directions for different H values agree well in both cases in Fig. 2 although the accuracy deteriorates with lag. The plotted semivariograms shows that the variance grows infinitely with lag distance for a medium described by a semivariogram given in Eq. 1.

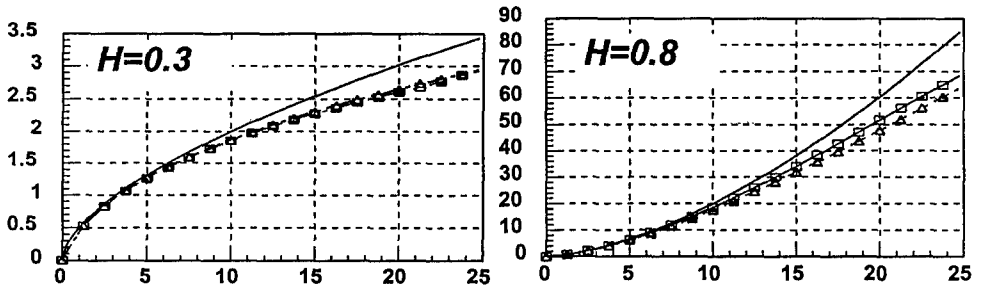

(a) $H = 0.3$ (b) $H = 0.8$

Figure 2: Simulated $\gamma_Y^{MC}(\mathbf{r})$ and theoretical $\gamma_Y(r) = a(r/\lambda)^{2H}$ semivariograms along NS and EW for fields in Figure (1).

3 Stochastic Finite Difference Flow Model

Steady-state confined flow of groundwater in a two-dimensional, horizontal, saturated, imcompressible porous medium with physical heterogeneity represented by simulated spatially varying fractal conductivity fields is considered in this study. Flow simulations were performed in a Monte Carlo manner for fractal fields of various H values. The simulation domain is a square domain where constant hydraulic heads are assigned at the left and right boundary and the no-flow condition on the top and bottom to create a uniform mean velocity $\bar{v}$. The numerical simulations are performed for fixed domain of $25\lambda \times 25\lambda$. Bellin *et al.*[7] suggest that flow and transport solutions are not affected by refinements of the grid size involving more than four points per integral scale λ. Here, we choose the following grid sizes in the longitudinal and transverse directions, $\Delta x = \Delta y = \lambda/4$.

Steady-state subsurface flow in the 2-d domain is described by

$$\nabla.\mathbf{q}(\mathbf{x}) = \nabla.\left(-K(\mathbf{x})\nabla\phi(\mathbf{x})\right) = 0 \tag{10}$$

where $\mathbf{q}(\mathbf{x})$ is the Darcy flux relative to the solid matrix and $\phi(\mathbf{x})$ is the hydraulic head. The flow equation is discretised by employing a mesh centered-finite difference scheme. The hydraulic heads at the nodal points are solved with the boundary conditions given above by a Gauss-Seidel method with successive over relaxation (SOR). In order to compute nodal heads, the interblock hydraulic conductivities are computed by geometric

averaging of adjacent conductivity values. This form of averaging ensures continuity of the head field and conservation of mass flux across block boundaries[17]. Darcy's law is applied to obtain the flux components $\mathbf{q}(\mathbf{x})$ and nodal velocities are computed by finite differencing with a constant porosity value of $\eta = 0.3$.

In order to check the accuracy and efficiency of the finite difference approximation of the flow equation, we calculated the local mass balance error which can be defined[18] as

$$e = (Q_{out} - Q_{in})/Q_{in} \times 100\% \tag{11}$$

where Q_{out} and Q_{in} are the total volume of flow out of the right boundary and into the left boundary, respectively. The mass balance error decreases when a smaller value of convergence criterion, μ, in the iterative scheme is used (the head changes in all nodes between two iterations is less than or equal to μ, iteration stops). We found that for each Monte Carlo simulation e is always less than 4% for each Hurst exponent H. These result, show that the finite difference solution is reasonably accurate, and accordingly, the obtained velocity field is sufficiently accurate to be used in the transport model. The mean velocity computed for Hurst exponent and with reference to 1500 Monte Carlo realisations was equal to unity leading to the conclusion that the mean velocity can indeed be assumed constant and unit in each realisation.

4 Stochastic Solute Transport Model

The random walk particle tracking method is commonly used in the field of statistical physics to model processes involving diffusion. This approach has also been used successfully to simulate reactive and non-reactive transport in the subsurface[4-7]. The basic idea is to approximate the spatial distribution of a transport quantity by a set of moving particles. The spatial location of particles are updated at each time step according to the following equation[23]

$$\mathbf{X}(t+\Delta t) = \mathbf{X}(t) + \left[\mathbf{V}(\mathbf{X},t) + \nabla \cdot \mathbf{d}(\mathbf{V}(\mathbf{X},t))\right]\Delta t + \left[2\mathbf{d}(\mathbf{V}(\mathbf{X},t))\Delta t\right]^{1/2} \cdot \mathbf{Z} \tag{12}$$

where $\mathbf{X}(t+\Delta t)$ is the updated position of the particle that was at $\mathbf{X}(t)$ in the previous step, $\mathbf{V}(\mathbf{X},t)$ is the velocity vector at the old position at time t, $\mathbf{d}$ is the local scale dispersion tensor, Δt is the time step, and $\mathbf{Z}$ is a vector of normally distributed random numbers of zero mean and unit variance. The second term on the right-hand side moves the particle advectively on the basis of the local velocity field at each point. The third term is important when stagnation regions or sharp fronts exist within the field[23]. The last term accounts for the local scale dispersion. The particle velocity needed in (12) is obtained by using a bilinear interpolation utilising the four velocity values surrounding the particle position. Eq. 12 is used to track 2000 non-interacting particles initially distributed along a strip of length 6λ normal to the mean flow direction of the domain. A constant dimensionless time step $\Delta t' = 0.05$ was chosen such that the fraction of the cell's length

traversed by a particle in a single time step is much smaller than one. The dimensionless time is given by $t' = \bar{v}t/\lambda$. The particle tracking experiments are performed in the inner core of the flow domain that is not affected by the boundaries. Particle tracking is terminated during each Monte Carlo run before the contaminant plume exits the inner core of the modelled domain.

5 Results from Flow and Transport Stochastic Analyses

Numerical generation of synthetic hydraulic conductivity fields, flow computations and transport simulations were carried out in a Monte Carlo manner for each Hurst exponent H. The simulation was terminated when the convergence criteria given in (9) were satisfied. For each Hurst exponent at least 1500 Monte Carlo runs were required to attain convergence. Numerical analyses were then carried out to calculate mean statistical quantities of interest from the flow and transport simulations.

Bellin *et al.*[7] show that the presence of boundaries influences the hydaulic head and velocity variabilities in two-dimensional domains. In Fig. 3, we plot results for the head variances σ_H^2 for different values of H averaged over 1500 Monte Carlo realisations. The head variability assumes a parabolic shape for each value of H. The parabolic shape of the curves reflects the statistical heterogeneity of the standard deviation in hydraulic head due to the constant head values specified on the boundaries of the flow domain. The head variance is zero at the fixed boundaries as expected and increases at the centre of the domain where it is maximum. The variance of hydraulic head σ_H^2, increases with H.

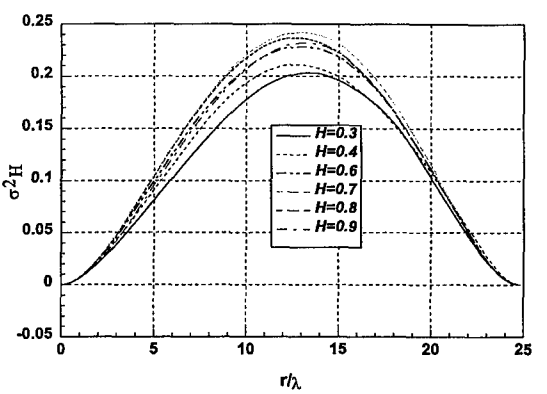

Figure 3: Head Variance σ_H^2 along the Longitudinal Axis for different values of H.

Figs. 4a and 4b show the average Monte Carlo longitudinal velocity variance σ_V^2 along the center line in the longitudinal direction (dashed curve), and also the center line along the transverse direction (solid curve), for $H = 0.4$ and 0.8 respectively.

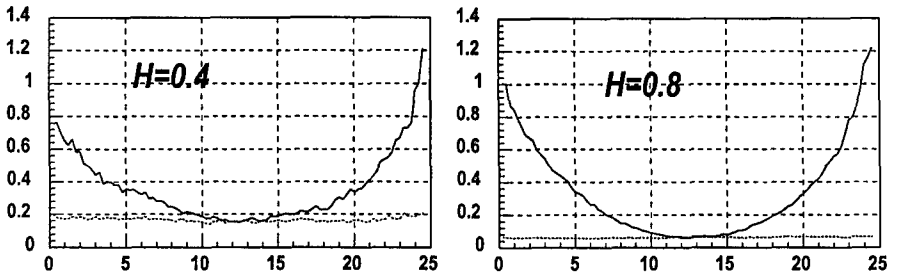

(a) (b)

Figure 4: Velocity Variance σ_V^2 Along the Centreline in the Longitudinal (Dashed) and Transverse (Solid) Direction.

While in the longitudinal direction σ_V^2 is nearly constant, in the transverse direction it assumes a parabolic shape. The longitudinal velocity variance is maximum at the impervious boundaries and decreases in transverse direction with distance from the boundaries reaching the minimum value at the domain centre.

Travel time statistics are important[7] because they are robust in characterising the dispersion process blending all sources of uncertainty into a unique curve. Fig. 5 illustrates travel time statistical distributions (breakthrough curves) at three distinct absorbing barriers placed normal to the mean flow respectively at distances 5λ, 10λ, and 15λ computed by counting the number of particles the cross each barrier for each transport simulation time. The figure is the average of 1500 Monte Carlo simulations for the case $H = 0.7$. This result shows that as the plume travels further from the contaminant source, the increased spreading of the plume results in both a corresponding attenuation and reduction in peak value of the breakthrough curves.

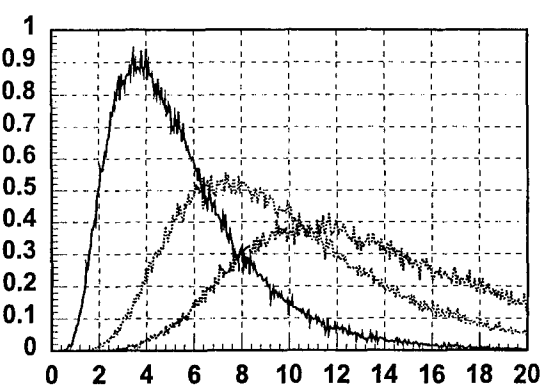

Figure 5:Travel Time Statistics for $H = 0.7$.

At the end of each Monte Carlo run, the moments of the dispersing plume are computed as follows: (a) the trajectory of the plume centroid:

$$R_i^m(t) = \frac{1}{N_p} \sum_{p=1}^{N_p} X_i^{m,p}(t), \tag{13}$$

where $X_i^{m,p}(t)$ ($i = 1,2$) are the coordinates of the p-th particle for the realisation m and N_P is the total number of particles; (b) the second-order central plume moment:

$$S_{ij}^m(t) = \frac{1}{N_p - 1} \sum_{p=1}^{N_p} \left[X_i^{m,p}(t) - R_i^m(t) \right] \left[X_j^{m,p}(t) - R_j^m(t) \right] \tag{14}$$

The moments (13) and (14) represent the overall plume behaviour in each one of the (equally probable) log conductivity fields. Average trajectories $\langle R_i(t) \rangle$, and the average of the second spatial moments $\langle S_{ij}(t) \rangle$ are obtained by taking expectations over MC independent Monte Carlo realisations:

$$\langle R_i(t) \rangle = \frac{1}{MC} \sum_{m=1}^{MC} R_i^m(t) \tag{15}$$

$$\langle S_{ij}(t) \rangle = \frac{1}{MC} \sum_{m=1}^{MC} S_{ij}^m(t) . \tag{16}$$

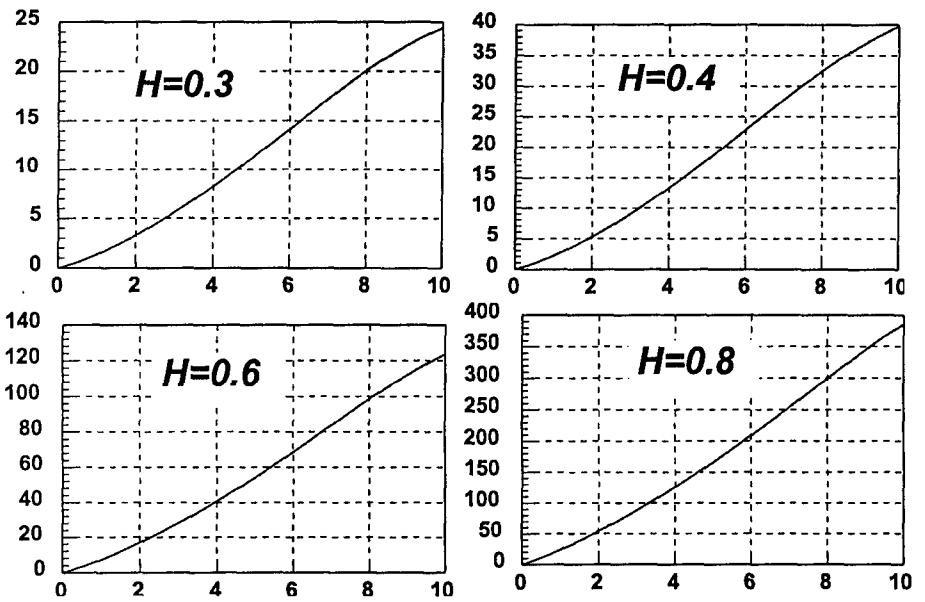

Figure 6: Particle Displacement Covariances $\langle S_{11}(t) \rangle - S_{11}(0)$ against $t' = \bar{v}t/\lambda$ for different values of H.

The expected values (15) and (16) represent the most probable estimate of the actual plume behaviour. Fig. 6 represents the average of 1500 simulated longitudinal second spatial moments $\langle S_{11}(t) \rangle - S_{11}(0)$ as a function of the dimensionless time $t' = \bar{v}t/\lambda$ for various values of H. Several observations can be made; as the value of the Hurst

exponent increases the second spatial moment increases with dimensionless time, a result that is consistent with the findings of Hassan *et al.*[5]. For each value of the Hurst exponent the second spatial moment increases non-linearly (non-Fickian) for all simulation times. This result can be explained by the fact that as the solute migrates in the porous medium, it continuously encounters spatially evolving scales of heterogeneity (fractal), hence the dispersion remains non-Fickian for all length scales below the scale of heterogeneity of the modelled domain (upper fractal cut-off scale R).

6 Summary

A two-dimensional numerical fractal-based Monte Carlo simulation model is developed to study flow and transport in heterogeneous media of spatially evolving heterogeneity. Realisations of the log fluctuating conductivity field are generated from a fractal or non-stationary distribution. The long range correlation of the hydraulic conductivity field is evident in the numerically obtained semivariograms. The flow simulations are carried out by solving a finite difference equation over a two-dimensional domain with uniform mean flow in one direction. The velocity field obtained from the conductivity realisations exhibits long range correlations. A random walk particle tracking technique is used to solve the solute transport problem for non-reactive solutes. The transport simulations indicate that higher Hurst exponent H (more persistence) of log conductivity results in more longitudinal spreading of the contaminant plume. Results also show that irrespective of the Hurst exponent the transport process is non-Fickian at all times for a dispersion process below the upper fractal cut-off scale R.

References

1. Gelhar, L. W. (1993). *Stochastic Subsurface Hydrology*. Prentice-Hall, Englewood Cliffs, New Jersey.
2. Rubin, Y. (1990). Stochastic analysis of macrodispersion in heterogeneous porous media. *Water Resources Research*, 26(1), 133-141.
3. Smith, L. and Freeze, R. A. (1979). Stochastic analysis of steady state groundwater flow in a bounded domain. 2. Two-dimensional simulations. *Water Resources Research*, 15(6), 1543-1559.
4. Smith, L., and Schwartz, F. W. (1980). Mass transport 1. A stochastic analysis of macroscopic dispersion. *Water Resources Research*, 16(2), 303-313.
5. Hassan, A. E., Cushman, J. H., and Delleur, J. W. (1997). Monte Carlo studies of flow and transport in fractal conductivity fields: Comparison with stochastic perturbation theory, *Water Resources Research,* 33(11), 2519-2534.
6. Bellin, A., Pannone, M., Fiori, A., and Rinaldo, A. (1996). On transport in porous formations characterised by heterogeneity of evolving scales. *Water Resources Research*, 32(12), 3485-3496.
7. Bellin, A., Salandin, P., and Rinaldo, A. (1992). Simulation of dispersion in heterogeneous porous formations: Statistics, first-order theories, convergence of computations. *Water Resources Research*, 28(9), 2211-2227.

8. Dagan, G. (1990). Transport in heterogeneous porous formations: Spatial moments, ergodicity, and effective dispersion. *Water Resources Research*, 26(6), 1281-1290.
9. Gelhar, L. W., and Axness, C. W. (1983). Three-dimensional stochastic analysis of macrodispersion in aquifers. *Water Resources Research,* 19(1), 161-180.
10. Sudicky, E. A. (1986). A natural gradient experiment on solute transport in a sand aquifer: Spatial variability of hydraulic conductivity and its role in the dispersion process. *Water Resources Research*, 22(13), 2069-2082.
11. Zhan, H., and Wheatcraft, S. W. (1996). Macrodispersivity tensor for non-reactive solute transport in isotropic and anisotropic fractal porous media: Analytical solutions. *Water Resources Research*, 32(12), 3461-3474.
12. Burrough, P. A. (1983). Multiscale sources of spatial variation in soil. I. The application of fractal concepts to nested levels of soil variation. *Journal of Soil Science*, 34, 577-597.
13. Molz, F. J., and Boman, G. K. (1995). Further evidence of fractal structure in hydraulic conductivity distributions. *Geophysical Research Letters,* 22(18), 2545-2548.
14. Kemblowski, M. W., and Wen, J. C. (1993). Contaminant spreading in stratified soils with fractal permeability distribution. *Water Resources Research*, 29(2), 419-425.
15. Neuman, S. P. (1990). Universal scaling of hydraulic conductivities and dispersivities in geologic media. *Water Resources Research,* 26(8) 1749-1758.
16. Mandelbot, B. B. (1983). *The Fractal Geometry of Nature.* W. H. Freeman, San Francisco.
17. Romeu, R.K., and Noetinger, B. (1995). Calculation of internodal transmisivities in finite difference models of flow in heterogeneous porous media. *Water Resources Research*, 31(4), 943-959.
18. Chin, D. A., and Wang, T. (1992). An investigation of the validity of first-order stochastic dispersion theories in isotropic porous media. *Water Resources Research*, 28(6), 1531-1542.
19. Mantoglou, A., and Wilson, J. L. (1982). The turning bands method for simulation of random fields using line generation by a spectral method. *Water Resources Research*, 18(5), 1379-1394.
20. Yin, Z. M. (1996). New methods for simulation of fractional Brownian motion. *Journal of Computational Physics*, 127, 66-72.
21. Addison P.S. and Ndumu A.S. (1999), 'Engineering Applications of Fractional Brownian Motion: Self-Similar and Self-Affine Random Processes', *Fractals,* 7(2), 151-157.
22. Addison P.S. (1997), *Fractals and Chaos: An Illustrated Course*, Institute of Physics Publishing, Bristol.
23. Tompson, A. F. B., and Gelhar, L. W. (1990). Numerical simulation of solute transport in three-dimensional randomly heterogeneous porous media. *Water Resources Research,* 26(10), 2541-2562.
24. Voss, R. F. (1989). Random fractals: Self-affinity in noise, music, mountains, and clouds. *Physica D*, 38, 362-371.